Bone Reports 15 (2021) 101088

Contents lists available at ScienceDirect

Bone Reports

journal homepage: www.elsevier.com/locate/bonr

Axial mechanical loading to *ex vivo* mouse long bone regulates endochondral ossification and endosteal mineralization through activation of the BMP-Smad pathway during postnatal growth

Satoshi Miyamoto [a], Hideki Yoshikawa [a], Ken Nakata [b,*]

[a] *Department of Orthopaedic Surgery, Osaka University Graduate School of Medicine, Yamadaoka 2-2, Suita, Osaka 565-0871, Japan*
[b] *Medicine for Sports and Performing Arts, Department of Health and Sport Sciences, Osaka University Graduate School of Medicine, Yamadaoka 2-2, Suita, Osaka 565-0871, Japan*

ARTICLE INFO

Keywords:
Mechanical loading
Bone mineralization
Endochondral ossification
Bone morphogenetic protein 2

ABSTRACT

Mechanical loading contributes to bone development, growth, and metabolism. However, the mechanisms underlying long bone mineralization *via* changes in loading during the growth period are unclear. The aim of the present study was to investigate the regulatory mechanisms underlying endochondral ossification and endosteal mineralization by developing an *ex vivo* organ culture model with cyclic axial mechanical loads. The metacarpal bones of 3-week-old C57BL/6 mice were exposed to mechanical loading (0, 7.8, and 78 mN) for 1 h/day for 4 days. Histomorphometry revealed that axial mechanical loading regulated the thickness of the calcified zone in the growth plate and endosteal mineralization in the diaphysis in a load-dependent manner. Mechanical loading also resulted in load-dependent upregulation of endochondral ossification and bone mineralization-related genes, including bone morphogenetic protein 2 (*Bmp2*). Recombinant human BMP-2 administration caused similar changes in tissue structures. Conversely, inhibition of the BMP-Smad pathway diminished the stimulatory effects of mechanical loading and BMP-2 administration, suggesting that the effects of mechanical loading may be exerted through activation of the BMP-Smad pathway with the results of gene ontology and pathway analyses. Mechanical loading increased alkaline phosphatase activity and decreased carbonic anhydrase IX (*Car9*) mRNA expression, resulting in a significant pH increase in the culture supernatant. We hypothesize that, through activation of the BMP-Smad pathway, mechanical loading downregulates *Car9*, which may alkalize the local milieu, thereby inducing bone formation and long bone mineralization. Our results showed that cyclic axial mechanical loading increased endochondral ossification and endosteal mineralization in developing mouse long bones, which may have resulted from changes in the pH, ALP activity, and Pi/PPi of the extracellular environment. These findings advance our understanding of the regulation of mineralization mechanisms by mechanical loading mediated through activation of the BMP-Smad pathway.

1. Introduction

Mechanical loading is an important regulator of bone growth, development, and metabolism, and appropriate mechanical stimulation is a key promoter of bone mineralization, specifically during endochondral ossification in the epiphyses (Sergerie et al., 2011; Ménard et al., 2014) and endosteal bone mineralization in the diaphysis (Sugiyama et al., 2012; Birkhold et al., 2016) of long bones. Numerous studies have described the effects of mechanical loading using various loading modalities (Simske et al., 1990; Turner et al., 1991; Moalli et al., 2000; Robling et al., 2001; De Souza et al., 2005; Zhang et al., 2006) and experimental models (Gluhak-Heinrich et al., 2003; Niehoff et al., 2004; Sundaramurthy and Mao, 2006; Robling et al., 2008; Moustafa et al., 2009; Saunders et al., 2010; Sergerie et al., 2011). However, the response of the growth plate to mechanical stimulation remains controversial, as different experimental designs and loading conditions have yielded different results (Ohashi et al., 2002; Niehoff et al., 2004; Sergerie et al., 2011; Ménard et al., 2014). Notably, few studies have employed an *ex vivo* model of an entire long bone exposed to cyclic axial mechanical loading.

* Corresponding author at: Medicine for Sports and Performing Arts, Department of Health and Sport Sciences, Osaka University Graduate School of Medicine, Yamadaoka 2-2, Suita, Osaka 565-0871, Japan.
E-mail addresses: miyamoto-s@ort.med.osaka-u.ac.jp (S. Miyamoto), yhideki@chp.toyonaka.osaka.jp (H. Yoshikawa), ken-nakata@umin.ac.jp (K. Nakata).

https://doi.org/10.1016/j.bonr.2021.101088
Received 3 December 2020; Received in revised form 19 March 2021; Accepted 1 May 2021
Available online 7 May 2021

Multiple studies have indicated that during cortical bone formation, the osteogenic response to mechanical loading is sensed and mediated by osteocytes and results from activation of the Wnt signaling pathway (Tatsumi et al., 2007; Bonewald and Johnson, 2008; Robling et al., 2008; Tu et al., 2012; Iura et al., 2015). However, signaling pathway analysis based on a genome-wide study predicted that additional signaling pathways may be involved in bone responses to mechanical loading (Zhang et al., 2009). Specifically, mechanical strain could promote osteoblast differentiation through the BMPs/Smad signaling pathway *via* the suppression of Smurf1 (Wang et al., 2010). Mechanical signals are integrated into the BMP signaling pathway within the Smad pathway, which suggests direct crosstalk of mechanotransduction and BMP signaling (Kopf et al., 2012). In addition, cyclic mechanical compression significantly upregulates BMP2 expression and results in osteogenesis *via* mechano-regulated autocrine signaling (Schreivogel et al., 2019). Therefore, BMP-induced Smad signaling could be involved to alter a cascade of mechanical strain or compression and its signal transduction to be mediated by having close relationships. However, the roles of the BMP-Smad pathway and its downstream targets in long bone growth and mineralization in response to mechanical loading are not well understood.

In the present study, we explored the regulatory mechanisms that give rise to endochondral ossification and endosteal mineralization in response to axial mechanical loading during postnatal growth, by assessing the role of the BMP-Smad signaling pathway and its potential downstream effects. We used a novel *ex vivo* model that involves cyclic axial loading to the entire long bones in a load-dependent manner, which allows to exclude the influence of *in vivo* systemic factors and to focus on the local microenvironment.

Endochondral ossification in the growth plate in response to mechanical loading was investigated in a different mechanical cyclic loading *ex vivo* condition as compared with articular cartilage, which is a hyaline cartilage similar to the growth plate cartilage, but does not undergo endochondral ossification because of permanent cartilage. In addition, to estimate phenotypic change in endochondral ossification in a load-dependent manner, not only the number of hypertrophic chondrocytes and uncalcified zones (cartilage) but also the calcified zones (cartilage calcification) of the growth plate were measured in undecalcified bone sections. With regard to endosteal bone mineralization, bone forming region from the mineralization front to the mineralized fluorochrome label and osteoid thickness in response to the *ex vivo* loading were evaluated. Whether the change in *ex vivo* mechanical loading drastically altered the extracellular fluid environment of the surrounding long bone was examined based on changes in pH, alkaline phosphatase (ALP) activity, and inorganic phosphate/pyrophosphate (Pi/PPi) levels in the supernatant. Subsequently, genome-wide screening of gene expression and pathway analyses were performed to identify long bone tissue-specific and mechanical loading-responsive genes using the *ex vivo* organ culture model, and a pathway and cascade associated with highly expressed genes was revealed, which enabled the extraction of multiple genes of interest associated with ossification. Furthermore, by inhibiting specific molecules and pathways related to potential targets, the underlying molecular mechanism of the promotion of mineralization *via* the activation of their signaling pathways was elucidated. Consequently, in the present study, we were able to investigate the regulation of mineralization in response to loading, identify molecules and pathways activated in response to the loading, and clarify their roles in bone growth and development, using an *ex vivo* model.

2. Materials and methods

2.1. Ex vivo organ culture model to achieve axial mechanical loading on mouse long bone

The forelimb bones of 3-week-old female and male C57BL/6 mice (average body weight 8.02 ± 0.26 g; Japan SLC Inc., Shizuoka, Japan), namely the fourth metacarpals from each mouse, were excised and processed for organ culture, yielding six metacarpal bones per experimental group (n = 6), and subjected to 0 mN, 7.8 mN, and 78 mN loadings. For organ culture, an insertion hole for a long bone sample was created at the midpoint of an atelocollagen sponge (φ = 5 mm, height = 3 mm; MIGHTY, Koken Co., Tokyo, Japan) using a 22-gauge piercing needle (φ = 0.71 mm). The sponge was soaked in organ culture medium (80 μl impregnated medium), and the metacarpals were then embedded vertically in a penetrating state until they were level with the bottom surface of the sponge (Supplementary Fig. 1A, C). Metacarpals with collagen sponges were cultured in separate wells of a 96-well culture plate, and the culture medium was changed every 24 h. Each well contained 0.2 ml MEM-alpha (Thermo Fisher Scientific, Inc., Waltham, MA, USA) supplemented with 0.2% bovine serum albumin (BSA; Sigma-Aldrich, St. Louis, MO, USA), 0.05 mg/ml ascorbic acid (Thermo Fisher Scientific, Inc., MA, USA), 1 mM sodium glycerophosphate (Sigma-Aldrich), and penicillin-streptomycin solution (Thermo Fisher Scientific) containing 100 U/ml penicillin and 100 mg/ml streptomycin, as previously reported (De Luca et al., 2001).

To understand the role of BMP-2 in the mineralization of long bones, we compared the effect of mechanical loading with that of recombinant human BMP-2 (rhBMP-2) administration. A single dose of 100 or 500 ng/ml rhBMP-2 (Osteopharma Inc., Osaka, Japan) was administered as an alternative to mechanical loading. To assess the role of BMP-Smad signaling following mechanical loading, dual Smad inhibition medium (Chambers et al., 2009), comprising organ culture medium with 10 nM TGF-β inhibitor (SB431542, Cayman Chemical Co., Inc., Ann Arbor, MI, USA) and 500 ng/ml noggin (Peprotech, Rocky Hill, NJ, USA), was used. In particular, TGF-β signaling *via* Smad2/3 is potentially activated to compensate for blockade of BMP-Smad signaling by Noggin. Therefore, SB431542, TGF-β/Smad inhibitor was used to eliminate its compensatory effect.

The experimental timeline and the design of the organ culture model with *ex vivo* mechanical loading are shown in Supplementary Fig. 1A–E. During organ culture, cyclic axial loading (0.5 Hz for 1 h/day for 4 days) was applied to the distal edge of metacarpals along their long axis (as close to this direction as possible), such that the mesial edge was stably supported on the bottom inner surface of the plate, using a custom-designed apparatus, a cyclic load bioreactor (CLS-5J-Z, Technoview, Osaka, Japan) (Supplementary Fig. 1B, C, E), as described previously (Muroi et al., 2007; Akamine et al., 2012; Shimomura et al., 2014). All specimens were incubated (37 °C, 5% CO_2) for 24 h prior to the application of cyclic load stimulation. Loads of three different magnitudes, equivalent to the entire body weight (8.0 g) or 1/10 (0.8 g) of the average body weight of 3-week-old mice, were as follows: 0 mN (improbable), 7.8 mN (appropriate), and 78 mN (excessive load) (Supplementary Fig. 1D). All research procedures involving animals were performed in accordance with the Laboratory Animals Welfare Act, the Guide for the Care and Use of Laboratory Animals, and the Guidelines and Policies for Rodent Experiments provided by the Institutional Animal Care and Use Committee (IACUC) at the Osaka University Graduate School of Medicine. In addition, all research procedures involving animals were approved by the IACUC. The protocol was approved by the Committee on the Ethics of Animal Experiments of the Osaka University Graduate School of Medicine (permit number: 27-086-000).

2.2. Histomorphometric analyses

Prior to metacarpal extraction (day 0; Supplementary Fig. 1D), tetracycline hydrochloride and calcein were administered to mice at 2 weeks after birth by intraperitoneal injection on days −6 (20 mg/kg tetracycline, Sigma-Aldrich) and −4 (16 mg/kg CL, Sigma-Aldrich). After organ culture for 6 days, with or without axial mechanical loading for 4 days or BMP administration, metacarpals were fixed in 70% ethanol and were subjected to Villanueva bone staining without

decalcification (Villanueva and Frost, 1961). The undecalcified bones were stained for 7 days, dehydrated in ethanol, and embedded in methylmethacrylate (Wako, Osaka, Japan). Frontal sections (5-μm thick) of the metacarpal body were cut from the undecalcified specimens using a microtome, and cross-sections (10-μm thick) of metacarpals were prepared as undecalcified polished specimens *via* a grinding process at Ito Bone Histomorphometry Institute (Niigata, Japan). All bone sections were subjected to histomorphometric analyses under a light microscope (BX-53, Olympus, Tokyo, Japan) using an image analyzer (System Supply Co., Nagano, Japan) by S. M. at the Institute. The magnification power of the microscope was 400×, and histomorphometric parameters were measured in an area of 0.0625 mm^2 (0.25 × 0.25 mm) in the central region of the growth plate and articular cartilage, equivalent to approximately 1/3 the width of the distal epiphysis. The cross-sections of cortical bone were measured in the mid-diaphyseal region (Supplementary Fig. 1F).

Histomorphometric measurements were defined and performed as follows: the articular cartilage [cartilage thickness (μm), chondrocyte number (N/mm), subchondral bone thickness (μm)], growth plate [thickness of uncalcified zone (μm) from the end of the distal edge of cartilage to mineralization front, hypertrophic chondrocyte number (N/mm^2), MF-TC thickness: thickness (μm) of calcified zone from mineralization front to tetracycline labeling labeling], and the cortical bone [cortical width (μm), marrow area (mm^2), osteoid thickness (μm), MF–TC thickness: thickness (μm) from mineralization front to tetracycline labeling]. In particular, to provide the precise measurement points of a labeling band mid-point and the boundary line of the mineralization front were handled maintaining the same observation field by immediate switching between natural light and fluorescence microscopy (Supplementary Fig. 2). In the growth plate, the MF–TC thickness of the calcified zone was measured from the mineralization front to tetracycline labeling along the direction of the longitudinally calcified intercolumnar septae. In the cortical bone, MF–TC thickness was measured from the mineralization front to the tetracycline labeling along the capillary canaliculi towards periosteum from the mineralization front. Hypertrophic chondrocytes were defined as enlarged cell bodies with calcifying of the cartilage matrix of intercolumnar septum (Amizuka et al., 2012) (Supplementary Fig. 2). Therefore, hypertrophic chondrocyte numbers (N/mm^2) were counted in the calcified cartilage towards the metaphysis from mineralization front and divided by the range of the measured area of the growth plate. Osteoid osteocyte number (N/mm) was measured on the frontal sections and divided by the entire osteoid surface. The longitudinal growth rate (LGR; μm/day) of the growth plate was calculated by measuring the MF-TC thickness and dividing it by the elapsed time (12 days) from the initial tetracycline labeling to the end of organ culture. The daily mineral apposition rate (MAR; μm/day) on the diaphyseal cortical bone was calculated by measuring the MF-TC thickness and dividing it by 12 days.

2.3. Microarray analysis

After organ culture, bone tissues were crushed in QIAzol lysis reagent (Qiagen, Hilden, Germany) using vigorous shaking with beads. Eight of the fourth metacarpals were used per loading group. Total RNA was extracted using chloroform and 70% ethanol and purified using an RNA purification kit (Qiagen). The cRNAs were amplified, labeled, and hybridized to a SurePrint G3 Mouse Gene Expression Microarray 8 × 60 K oligomicroarray (Agilent Technologies, Santa Clara, CA, USA). All hybridized microarray slides were scanned, and relative hybridization intensities and background were calculated using the Agilent Feature Extraction Software (9.5.1.1) (Agilent Technologies). The raw signal intensities of samples were normalized using a quantile algorithm, and comparisons between control and experimental samples were made using the 'preprocessCore' library package [P] on Bioconductor software [B]. The analysis criteria (Quackenbush, 2002) for screening differentially expressed genes (DEGs) of long bone tissue-specific genes related to ossification and chondrocytes were as follows: upregulated genes, *Z*-score ≥ 2.0 and ratio ≥ 1.5-fold; down-regulated genes, Z-score ≤ −2.0 and ratio ≤ 0.66. Microarray experiments and analyses were performed at Cell Innovator Inc. at Kyushu University (Fukuoka, Japan).

To further investigate extracted DEGs, pathways and biological processes were analyzed using the gene ontology (GO) database (http://www.geneontology.org/page/go-database) and Kyoto Encyclopedia of Genes and Genomes (KEGG) database (http://www.genome.jp/kegg). Enrichment analysis was performed using a modified Fisher's exact test using the Database for Annotation, Visualization and Integrated Discovery (DAVID) Bioinformatics resource v6.8 (ttps://david.ncifcrf.gov); $p < 0.01$ was applied as the threshold.

2.4. Quantitative PCR

Total RNA isolation was performed as described above. First, a cDNA reverse transcription kit (Thermo Fisher Scientific) was used for cDNA synthesis. Quantitative PCR was performed using SYBR qPCR mix reagent (Toyobo Co., Osaka, Japan) and the StepOnePlus Real-Time PCR System (Applied Biosystems, Foster City, CA, USA). The comparative Ct method was used for quantitative data analysis, normalizing to *Gapdh* as an internal control. The primer sets used in this study are listed in Supplementary Table 1.

2.5. Analysis of extracellular fluid in the organ culture supernatant

Organ culture supernatants were assayed to examine how the cultured organs affected the extracellular fluids. The culture medium used for the measurement was a modified version of the organ culture medium described above that was free of glycerophosphate and ascorbic acid. At 24 h after mechanical loading (Supplementary Fig. 1D), pH changes in the culture supernatant were measured in 100 μl volumes using a pH/ion meter and pH electrode (F-72, 9618S-10D, Horiba, Kyoto, Japan). Additional supernatant samples of culture medium were stored at −80 °C for later measurement of ALP activity. For this, they were purified in 100% acetone at −20 °C overnight and incubated for 15 min at 37 °C; ALP activity was then measured at room temperature using LabAssay ALP (Wako). Inorganic phosphate (Pi) concentrations in the supernatant were measured using a Malachite Green Phosphate Assay (BioAssay Systems, Hayward, CA, USA). Inorganic pyrophosphate (PPi) levels were determined using an Inorganic Pyrophosphate Assay (Lonza, Basel, Switzerland) and a microplate luminometer (Centro XS3 LB960, Berthold Technologies, Bad Wildbad, Germany).

2.6. Immunohistochemistry

After organ culture, bone samples were fixed overnight in 10% neutral buffered formalin and decalcified in 10% EDTA for 2 h. They were embedded in paraffin, and 6-μm thick sections were cut and placed on microscope slides and then treated with methanol. After blocking with 5% BSA, sections were treated with a polyclonal anti-phospho-Smad 1/5/8 antibody (Cell Signaling Technology, Danvers, MA, USA) followed by staining with Alexa Fluor 488-labeled secondary antibody (Cell Signaling Technology). The nuclei were stained with Hoechst 33342 reagent (Dojindo Laboratories, Kumamoto, Japan), and sections were visualized using a confocal laser-scanning microscope (FluoView FV-1000, Olympus).

2.7. Western blotting

Metacarpal bones were harvested immediately after mechanical loading on day 1 (Supplementary Fig. 1D) and homogenized with beads in lysis buffer (#SN-002) with protease inhibitor cocktail phosphatase (Sigma-Aldrich) and phosphatase inhibitor cocktail (Nacalai Tesque, Kyoto, Japan) using a Minute protein extraction kit (Invent Biotechnologies, Plymouth, mN, USA). Eight metacarpal bones were used

per loading group. Equal amounts of total protein were loaded into each well and electrophoresed on 4–12% gradient polyacrylamide gels (Thermo Fisher Scientific) with SDS running buffer (Thermo Fisher Scientific) and transferred to a polyvinylidene fluoride (PVDF) membrane (Nippon Genetics, Tokyo, Japan). The membrane was blocked with 5% nonfat dry milk for 15 min in Tris-buffered saline with 0.1% Tween-20 (TBS-T) at 25 °C and incubated overnight with primary antibodies against Smad1, phospho-Smad1/5/8, Smad2/3, or phospho-Smad2/3 (Cell Signaling Technology) at 4 °C, followed by incubation with appropriate secondary horseradish peroxidase-conjugated antibodies (Cell Signaling Technology) at room temperature for 1 h. After washing each membrane with TBS-T, bound antibodies were visualized by enhanced chemiluminescence using Amersham ECL Prime Western Blotting Detection Reagent (GE Healthcare Life Sciences, Marlborough, MA, USA).

2.8. Statistical analysis

All data are presented as the mean ± standard deviation (SD). Group mean values were analyzed by the Tukey-Kramer test for multiple group comparisons. Results were considered statistically significant at $p < 0.05$. Analyses were performed using Microsoft Excel and Statcel3 (OMS Publishing, Saitama, Japan).

3. Results

3.1. Mechanical loading promotes endochondral ossification in the growth plate but not in articular cartilage

In articular cartilage, no significant changes in response to mechanical loading were observed in cartilage thickness or number of chondrocytes (Fig. 1A, D, E). Similarly, subchondral bone thickness did not change significantly in response to mechanical loading (Fig. 1F). In contrast, mechanical loading significantly increased the number of hypertrophic chondrocytes (Fig. 1B, C, G).

Both *in vivo* (with labeling prior to sacrifice) and *ex vivo* (in organ culture), the growth plate thickness included not only an uncalcified zone but also a calcified zone, defined histologically as a calcified cartilage and osseous zone from the mineralization front of the growth plate to the tetracycline-labeled osseous tissue. Mechanical loading significantly increased the thickness of the calcified zone (Fig. 2A, C) in the growth plate and decreased the thickness of the uncalcified zone (Fig. 2A, B) in a load-dependent manner (Supplementary Fig. 3). The LGR, an indicator of long bone growth, was 2.48 ± 0.23 μm/day, 3.72 ± 0.62 μm/day, and 4.31 ± 0.41 μm/day for loads of 0 mN, 7.8 mN (*vs.* 0 mN, $p < 0.01$), and 78 mN (*vs.* 0 mN, $p < 0.01$), respectively.

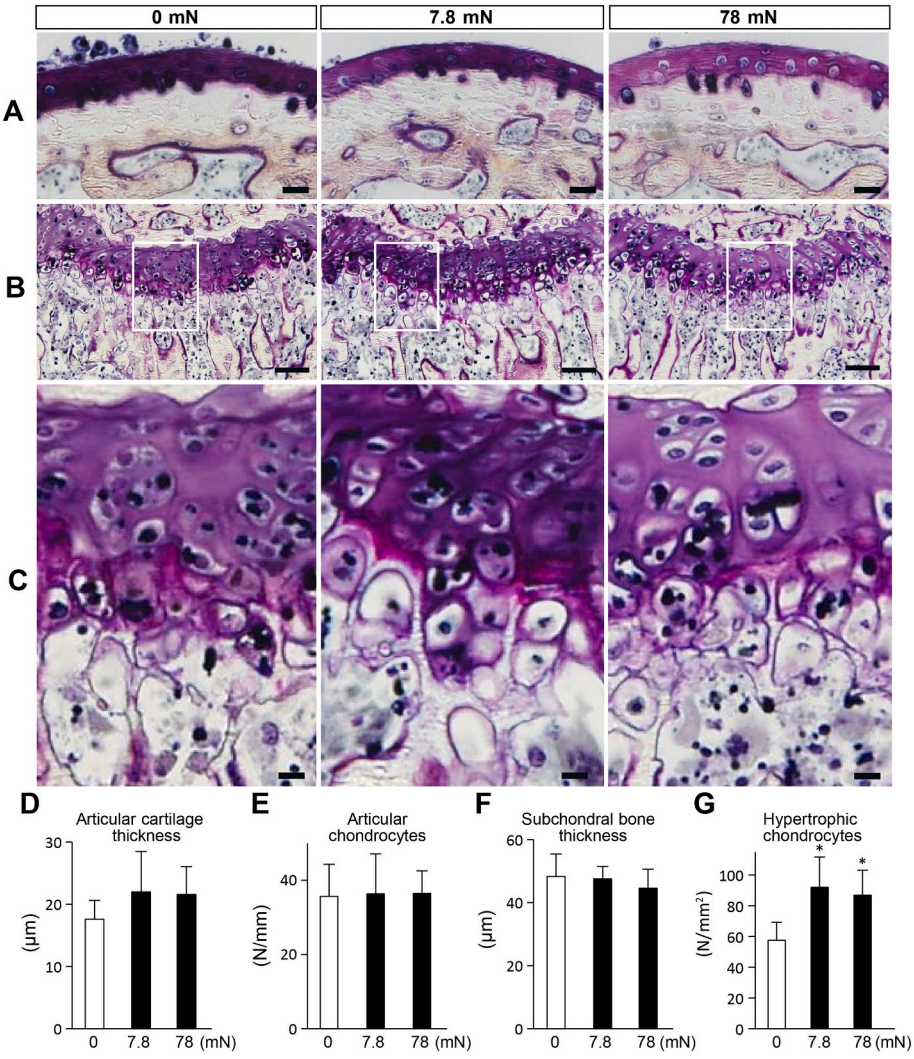

Fig. 1. Mechanical loading increased the number of hypertrophic chondrocytes in the subchondral bone, but not the number of articular chondrocytes in the articular cartilage. Frontal sections of the distal epiphysis of metacarpals subjected to Villanueva's bone staining. (A) Articular cartilage and subchondral bone. Scale bar = 20 μm. (B) Growth plate and metaphysis. Scale bar = 50 μm. (C) Hypertrophic chondrocytes in calcified cartilage. Scale bar = 10 μm. (D) Articular cartilage thickness (n = 6/group). (E) Number of articular chondrocytes (n = 6/group). (F) Subchondral bone thickness (n = 6/group). (G) Number of hypertrophic chondrocytes (n = 6/group). The bars represent the mean + SD. *$p < 0.05$, as determined by the Tukey-Kramer test for multiple comparisons.

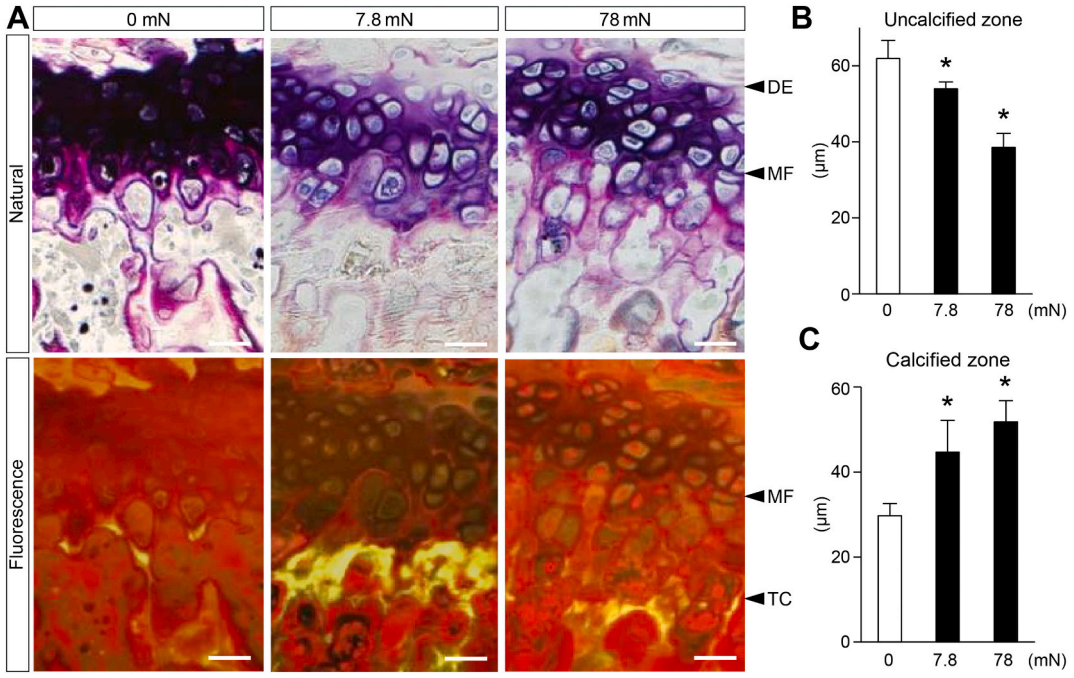

Fig. 2. Mechanical loading decreased the uncalcified zone thickness and increased the calcified zone thickness in the growth plate. Frontal sections of the distal epiphysis of metacarpals treated by Villanueva's bone staining. (A) Light (upper panel) and fluorescence (lower panel) microscopy images. Scale bar = 20 μm. (B) Thickness of the uncalcified zone from the end of the distal edge (DE) to the mineralization front (MF) (n = 6/group). (C) Thickness of the calcified zone from the MF to the beginning of the area positive for tetracycline (TC) labeling (n = 6/group). The bars represent the mean + SD. *p < 0.05, as determined by the Tukey-Kramer test for multiple comparisons.

3.2. Mechanical loading promotes endosteal bone mineralization

No significant differences in cortical width, marrow area, or osteoid thickness were observed in response to loading magnitude (Fig. 3A–D). In contrast, MF–TC thickness of the mineralization front to the tetracycline-labeled mineralized tissue increased significantly in response to loading (Fig. 3E), whereas osteoid thickness showed a slight but not significant increase with loading. The calculated MAR values were 2.67 ± 0.31 μm/day, 3.69 ± 0.67 μm/day, and 3.74 ± 0.45 μm/day under 0 mN, 7.8 mN (*vs.* 0 mN, $p < 0.01$), and 78 mN loading (*vs.* 0 mN, $p < 0.01$), respectively. Since the endosteal bone mineralization, namely the MF–TC thickness both *in vivo* (with labeling prior to sacrifice) and *ex vivo* (in organ culture), is included, it must be considered to consist of the mineralized bone produced in the past until the present over a period of 12 days.

3.3. Mechanical loading induces the expression of genes related to endochondral ossification and bone mineralization

When compared to gene expression levels under no load, similar

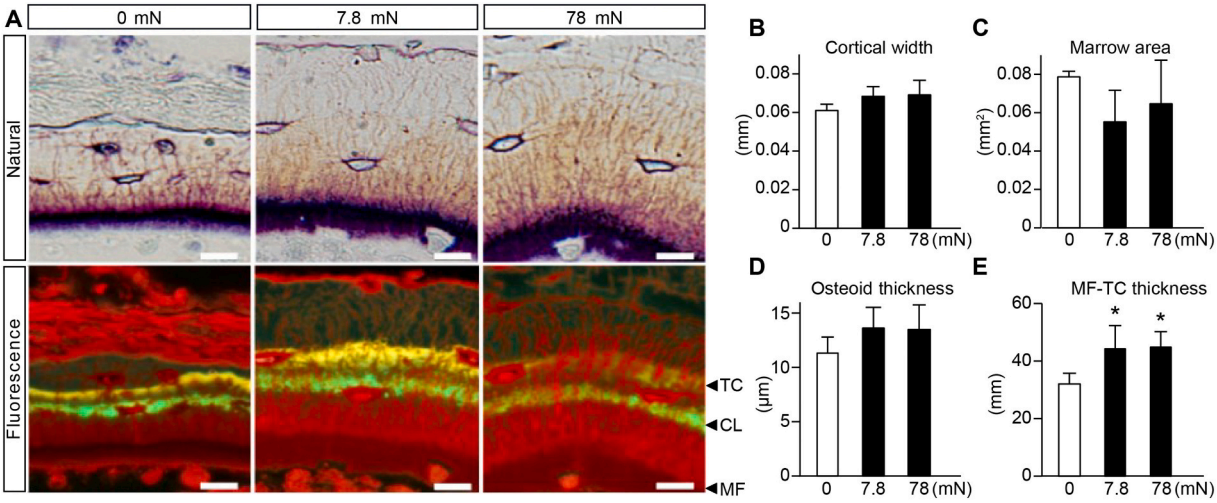

Fig. 3. Mechanical loading promoted endosteal bone mineralization. Cross-sections of cortical bone in the mid-diaphyseal region of metacarpals treated by Villanueva's bone staining. (A) Endosteal mineralization of undecalcified sections. Light (upper panel) and fluorescence (lower panel) microscopy images. Scale bar = 10 μm. (B) Cortical bone width of undecalcified sections, including the osteoid (n = 6/group). (C) Bone marrow area of undecalcified sections, including the osteoid (n = 6/group). (D) Osteoid thickness from the osteoid surface to the mineralization front (MF) (n = 6/group). (E) Thickness from the MF to the tetracycline (TC) labeling (n = 6/group). CL: calcein labeling. The bars represent the mean + SD. *p < 0.05, as determined by the Tukey-Kramer test for multiple comparisons.

gene expression profiles were observed with 7.8 and 78 mN loading, although several mRNAs were upregulated with 78 mN loading compared to levels under 7.8 mN loading (Fig. 4A). Among the extracted 93 response genes out of the 827 searched genes associated with chondrocytes and ossification based on GeneCards human gene database (https://www.genecards.org/) in microarray analysis, 37 genes were upregulated and 20 genes were downregulated in response to 7.8 mN loading (compared to 0 mN loading). Following 78 mN loading, 39 genes were upregulated and 39 genes were downregulated (compared to 0 mN loading) (Supplementary Fig. 3A, B, C). Mechanical loading upregulated the expression of genes involved in both endochondral ossification and bone mineralization in long bone tissue, such as *Ihh*, *Col10a1*, *Mmp13*, *Wnt4*, *Spp1*, *Dmp1*, *Mepe*, *Phex*, and *Bmp6* (Fig. 4B, C). The effects of mechanical loading on the regulation of gene expression in long bones were load-dependent. Intriguingly, we found that mechanical loading consistently downregulated carbonic anhydrase IX (*Car9*) and acid phosphatase 5 (*Acp5*) compared with levels in the non-loading group (Fig. 4A, B).

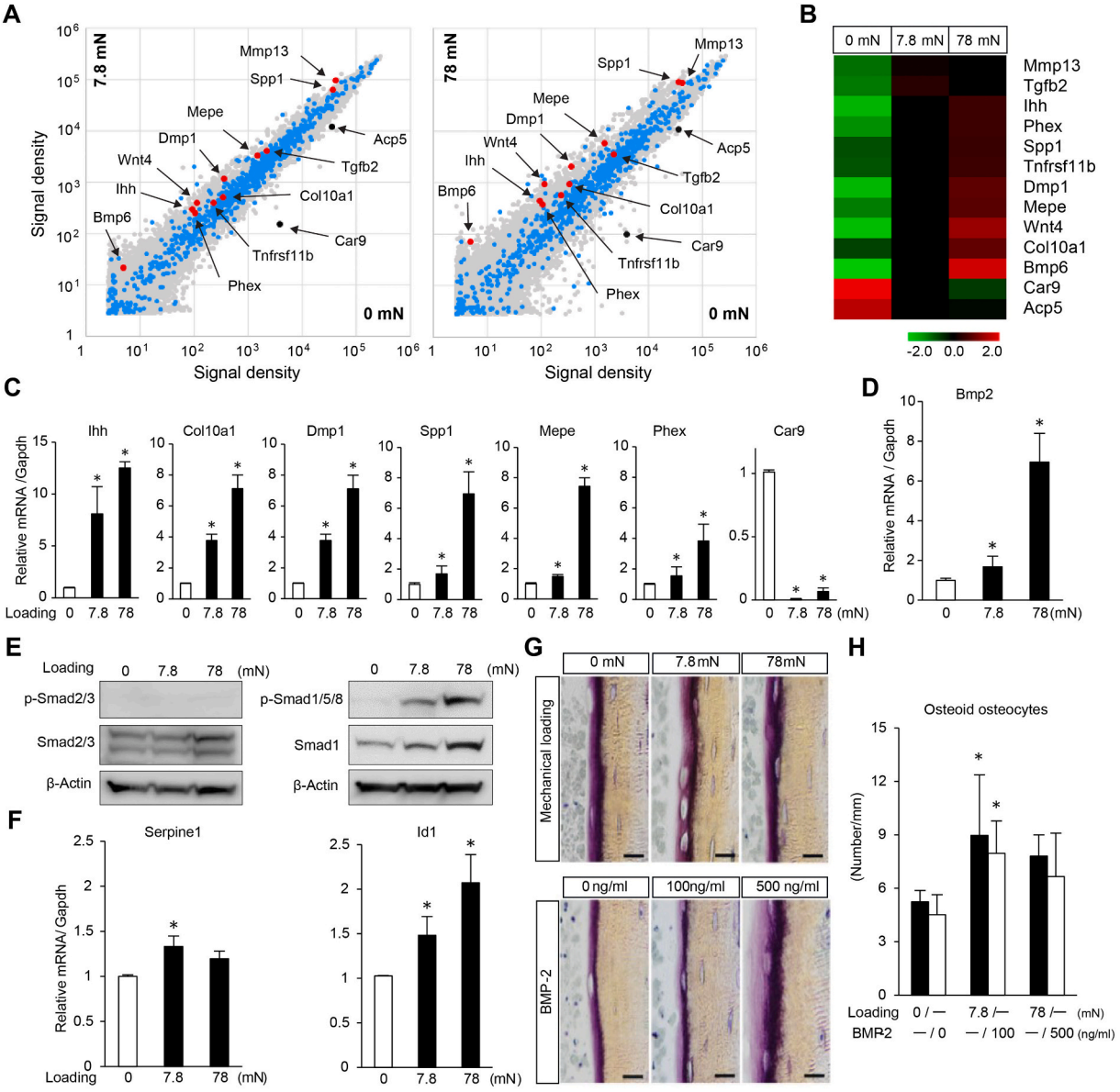

Fig. 4. Gene expression, Smad1/5/8 phosphorylation, and changes in the number of osteoid osteocytes occurring in response to mechanical loading. (A) Scatter plots of gene expression following load magnitudes of 7.8 or 78 mN (*versus* 0 mN), as determined by microarray analysis. Colored dots represent 827 searched chondrocyte- and ossification-related genes based on the GeneCards database (blue), and markedly upregulated (red) and downregulated (black) genes from the 93 extracted genes in response to the loading are indicated. (B) Heatmap showing the extracted genes that are indicated in the scatter plots in A. (C) The extracted mRNA expression levels of endochondral ossification and bone mineralization-related genes, as determined by quantitative reverse transcriptase-polymerase chain reaction (qRT-PCR) analysis. All results were normalized to that of *Gapdh* and are relative to the expression levels observed when the loading force was 0 mN (n = 3/group). (D) Mechanical loading increased BMP-2 expression (n = 3/group). (E) Mechanical loading induced the phosphorylation (p) of Smad 1/5/8, but not Smad2/3. Representative western blot showing the levels of p-Smad2/3 and p-Smad1/5/8 after mechanical loading at day 1. (F) Mechanical loading preferentially activated expression of the BMP-induced marker *Id1* over the TGF-β-induced marker *Serpine1* (encoding PAI-1). All mRNA expression levels determined by qRT-PCR analysis were normalized to that of *Gapdh* and are expressed relative to those observed when the loading force was 0 mN (n = 3/group). (G) Osteoid osteocytes on the endosteal surface upon mechanical loading (upper panel) and single BMP-2 administration (lower panel). (H) Mechanical loading and BMP-2 administration increased the number of osteoid osteocytes (n = 6/group). Scale bar = 10 μm. The bars represent the mean + SD. *p < 0.05, as determined by the Tukey-Kramer test for multiple comparisons.

GO and pathway analyses for screening DEGs were performed for long bone tissue in response to mechanical loading *ex vivo*. The key pathways, such as BMP signaling, epidermal growth factor receptor (EGFR/ErbB) signaling, and GO terms, including Smad phosphorylation, ossification, mitogen-activated protein kinase (MAPK) cascade, Cartilage development, calcium ion input, and phosphate metabolic were enriched in the screened DEGs and were demonstrated to be involved in long bone tissue responses to the increased loading. Based on the GO term and pathway screening results, the following top four pathways and cascades were identified: BMP/Smad signaling, EGFR/ErbB signaling, MAPK, and ossification. Therefore, although we focused on the role of BMP in comparison to that of *ex vivo* loading on long bone tissue, the effects of mechanical loading apparently increased cartilage ossification and bone mineralization, and we observed the changes not only in the form of the up-regulation of specific responsive genes related to cartilage and ossification but also preferential induction *via* the activation of BMP/Smad signaling (Supplementary Figs. 4, 5).

3.4. Mechanical loading activates BMP-Smad1/5/8 signaling-mediated endochondral ossification and endosteal mineralization

Based on the results of GO and pathway analyses, we observed significant increases in *Bmp2* gene expression that were load-dependent (Fig. 4D). For further analysis, we used antibodies against activated Smad proteins, which are key downstream effectors of the TGF-β and BMP signaling pathways. Smad2/3 phosphorylation was barely detectable in response to mechanical loading, but Smad1/5/8 phosphorylation appeared to be mediated by increased mechanical loading (Fig. 4E). Most cells in the growth plate and endosteum were positively labeled with phospho-Smad1/5/8 after 7.8 mN and 78 mN loading, but not after 0 mN loading (Supplementary Fig. 4). Regarding downstream targets of both pathways, the expression of *Serpine1* (encoding PAI-1, an inducible marker of TGF-β/Smad2/3) was relatively unchanged regardless of the load, whereas mechanical loading significantly increased the expression of *Id1*, which is induced by BMP/Smad1/5/8 signaling (Fig. 4F). Thus, our results showed that increased mechanical loading led to activation of BMP-Smad1/5/8 signaling during endochondral ossification and endosteal bone mineralization. We also found that mechanical loading and BMP-2 administration independently increased the number of osteoid osteocytes but not osteoid thickness (Fig. 4G, H).

3.5. Inhibition of BMP-Smad signaling diminishes cartilage calcification and reduces endochondral ossification

BMP-2 administration decreased the thickness of the uncalcified zone and increased that of the calcified zone in the growth plate in a dose-dependent manner (Fig. 5B, E, F). Thus, the action of BMP-2 in endochondral ossification closely resembles accelerated ossification by mechanical loading (Fig. 5A, C, D). Use of both the BMP antagonist noggin and the TGF-β/Smad inhibitor SB431542 to inhibit BMP-Smad signaling dramatically diminished not only the loading-induced

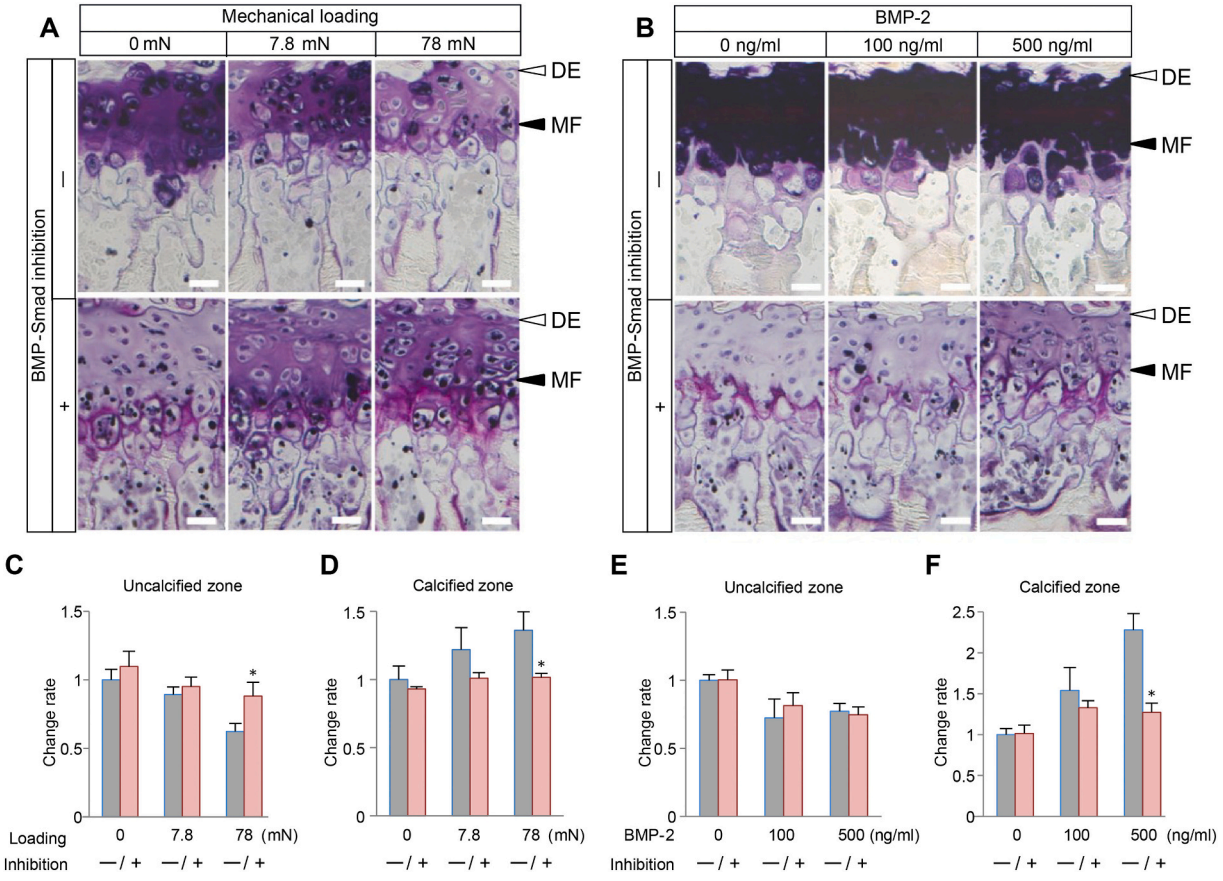

Fig. 5. Comparison of the effects of mechanical loading and BMP-2 administration, with or without BMP-Smad pathway inhibition, on the growth plates of undecalcified sections. White arrowheads show the end of the distal edge (DE), and black arrowheads show the mineralization front (MF). The regions between the arrowheads represent uncalcified zones. (A) Effects of mechanical loading, with or without BMP-Smad inhibition. Scale bar = 20 μm. (B) Effects of BMP-2 administration, with or without Smad inhibition. Scale bar = 20 μm. Rates of change in the thickness of uncalcified (C) and calcified (D) zones in growth plates after mechanical loading, with or without BMP-Smad inhibition (n = 6/group). Rates of change in the thicknesses of uncalcified (E) and calcified (F) zones in growth plates after BMP-2 administration, with or without BMP-Smad inhibition (n = 6/group). The bars represent the mean + SD. *p < 0.05, as determined by the Tukey-Kramer test for multiple comparisons.

reduction in the thickness of the uncalcified zone but also the loading-induced increase in the thickness of the calcified zone (Fig. 5C, D). By contrast, inhibition of BMP-Smad signaling seemed to have no impact on the BMP-2-induced reduction in the thickness of the uncalcified zone but did diminish the dose-dependent BMP-2-induced increase in the thickness of the calcified zone (Fig. 5E, F). The inactivation of BMP-Smad signaling may have been overcome by the high doses of BMP-2 and possibly also by the activation of alternative downstream signaling pathways; this hypothesis might explain the lack of a significant effect of BMP-Smad inhibition on the BMP-2-induced reduction in the thickness of the uncalcified zone of the growth plate.

3.6. Inhibition of BMP-Smad signaling reduces the region of mineralization and diminishes endosteal bone mineralization

Mechanical loading significantly increased the MF–TC thickness of the mineralization front to the tetracycline-labeled mineralized tissue (Fig. 6A, C, D). BMP-2 administration showed similar tendencies, with a significant increase in the MF–TC thickness, but only slight changes in osteoid thickness (Fig. 6B, E, F). Inhibition of BMP-Smad signaling diminished endosteal bone mineralization, particularly the MF–TC thickness, under baseline conditions and mechanical loading (Fig. 6D, F). Notably, the effects of inhibition of BMP-Smad signaling on the MF–TC thickness were overcome by BMP-2 administration.

3.7. Mechanical loading regulates the extracellular environment of long bones

Mechanical loading significantly increased the pH and ALP activity of the culture supernatant (Fig. 7A, B). Furthermore, mechanical loading markedly decreased PPi and increased Pi in the supernatant (Fig. 7C, D). The change in Pi/PPi ratio was 2.35 fold under 7.8 mN and 3.02 fold under 78 mN when compared to the ration under 0 mN loading ($p < 0.01$).

4. Discussion

Mechanical stimulation is an essential inducer of long bone growth and potentiates cartilage and bone matrix mineralization. However, it remains unclear how axial mechanical stimulation regulates mineralization. The present findings show that cyclic axial mechanical loading to *ex vivo* long bones may regulate endochondral ossification and endosteal bone mineralization by activating BMP-Smad signaling (Fig. 8). In this study, we used simple experimental conditions to analyze the mineralization changes induced in long bones by cyclic axial mechanical loading and employed an organ culture model to exclude systemic factors *in vivo* and to focus on the local milieu.

Previous studies have provided conflicting results regarding whether the growth plate thickness increases (Ohashi et al., 2002; Wang and Mao, 2002; Othman et al., 2007) or decreases (Alberty et al., 1993; Sergerie et al., 2011; Bries et al., 2012) in response to mechanical loading. In this study, histomorphometric analysis revealed that the

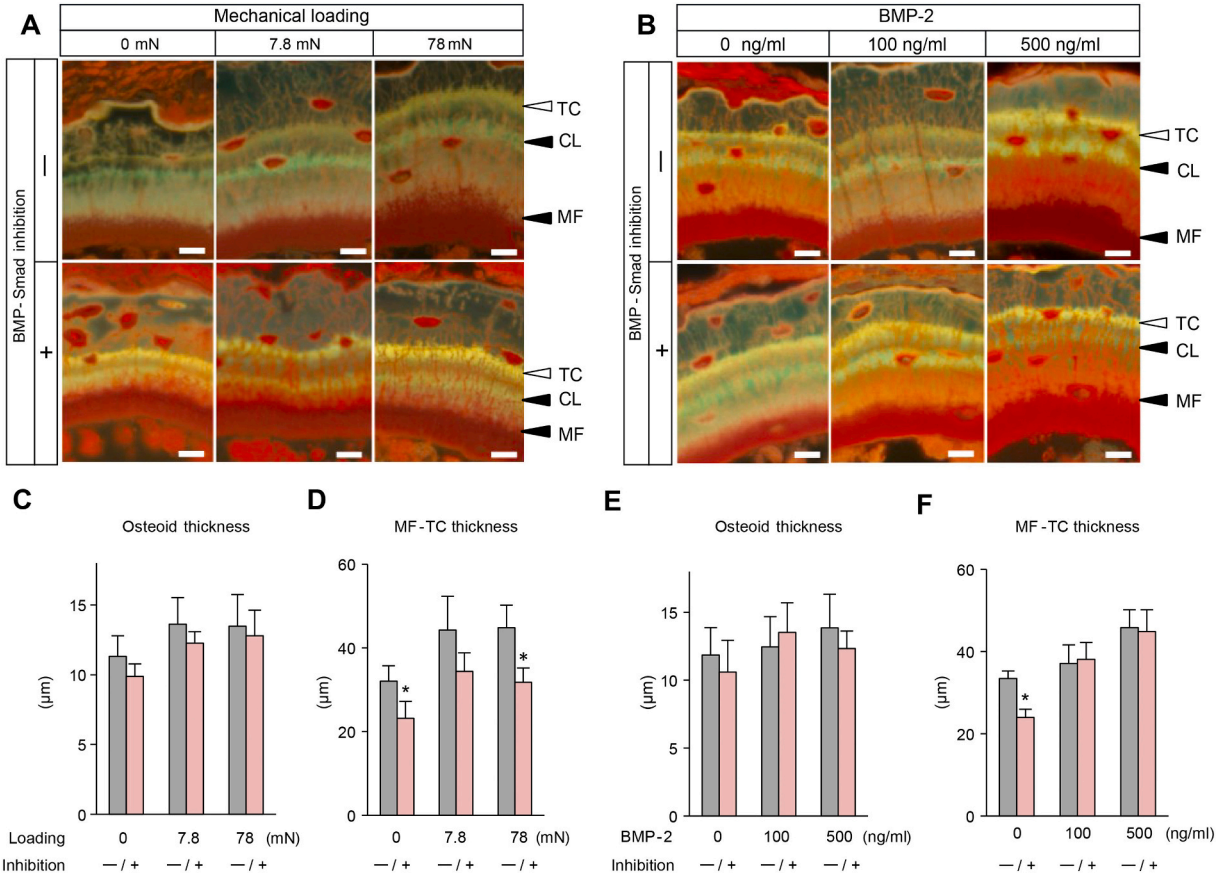

Fig. 6. Comparison of the effects of mechanical loading and BMP-2 administration, with or without BMP-Smad pathway inhibition, on endosteal bone mineralization in undecalcified sections. The arrowheads show tetracycline (TC) labeling, calcein (CL) labeling, and the mineralization front (MF). (A) Effects of mechanical loading with or without BMP-Smad inhibition. Scale bar = 10 μm. (B) Effects of BMP-2 administration with or without BMP-Smad inhibition. Scale bar = 10 μm. (C) Osteoid thickness and (D) MF–TC thickness after mechanical loading with or without BMP-Smad inhibition (n = 6/group). (E) Osteoid thickness and (F) MF–TC thickness after BMP-2 administration with or without BMP-Smad inhibition (n = 6/group). The bars represent the mean + SD. *$p < 0.05$, as determined by the Tukey-Kramer test for multiple comparisons.

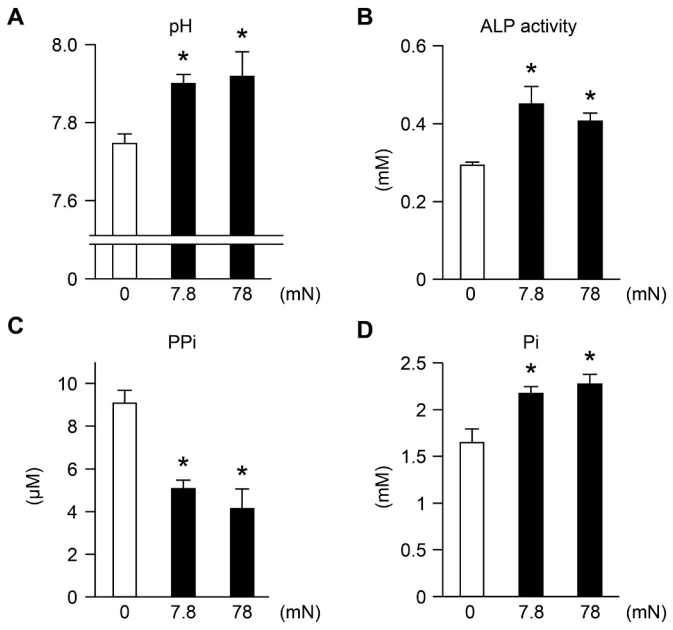

Fig. 7. Mechanical loading regulates the extracellular environment in the culture supernatant. (A) pH (n = 5/group). (B) Alkaline phosphatase (ALP) activity (n = 3/group). (C) Inorganic pyrophosphate (PPi) levels (n = 3/group). (D) Inorganic phosphate (Pi) levels (n = 3/group). The bars represent the mean + SD. *p < 0.05, as determined by the Tukey-Kramer test for multiple comparisons.

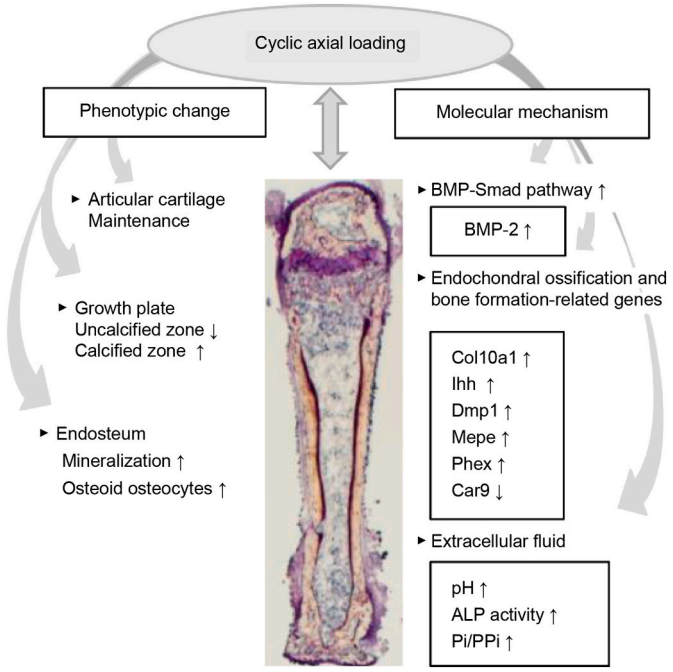

Fig. 8. Model of the roles of mechanical loading in the growth, development, and mineralization of the long bone. The model indicates that phenotypic changes and molecular mechanisms are regulated by mechanical loading during endochondral ossification and endosteal mineralization. We propose that mechanical loading might exert its effects by promoting alkalinization of the local milieu *via* activation of the BMP-Smad pathway.

thickness of the calcified and uncalcified zones in the growth plate increased and decreased, respectively, in a load-dependent manner and that these changes were not observed in articular cartilage. This is, to the best of our knowledge, the first report that the growth plate is much more sensitive in terms of chondral calcification in response to cyclic axial mechanical loading than is the articular cartilage, which does not undergo calcification during bone development. Regarding cortical bone mineralization, histomorphometry has revealed that *in vivo* mechanical loading increases bone formation (Zhang et al., 2006; Zhang et al., 2007; Kuruvilla et al., 2008; Sample et al., 2010; Weatherholt et al., 2013; Baumann et al., 2015). We demonstrated that *ex vivo* mechanical loading increases endosteal bone mineralization and the number of osteoid osteocytes. These results suggest that mechanical loading is essential not only for promoting initial primary mineralization, but perhaps also for mobilizing osteocytes from osteoblasts to increase subsequent bone matrix mineralization.

In this study, osteoid thickness did not vary significantly with changes in mechanical loading. The osteoid, which is the unmineralized bone matrix secreted by osteoblasts, may play a vital role in preventing excess mineralization by maintaining constant thickness.

BMP and TGF-β signaling play crucial roles in bone growth, development, and homeostasis; in addition to their indispensable role in bone formation, signal interplay and crosstalk between BMP and TGF-β regulate hypertrophic maturation of chondrocytes in endochondral ossification (Keller et al., 2011; Dexheimer et al., 2016). Moreover, previous studies have demonstrated that synergistic effects of TGF-β and BMP induce significant bone formation (Duneas et al., 1998; Simmons et al., 2004) and that TGF-β accelerates BMP function (Tachi et al., 2011). To assess the role of BMP-Smad signaling in response to mechanical loading in endochondral ossification, we inhibited BMP-Smad signaling under various conditions of mechanical loading, as well as administering exogenous BMP-2. However, the antagonist or opposite effect between the BMP and TGF-β pathways are recognized, having similar downstream transduction effectors and their regulation being closely related to the biological basis of their antagonistic interaction (Ning et al., 2019). Therefore, both the BMP antagonist noggin and the TGF-β type 1 receptor inhibitor SB431542 were used not only to block the BMP/Smad1/5/8 signaling but also eliminate the activation of TGF-β/Smad2/3 signals induced by the suppression of the BMP pathway, an approach widely employed for dual Smad inhibition (Chambers et al., 2009).

Based on the GO and pathway analyses results, mechanical loading activated BMP-Smad signaling, and the mode of action of mechanical loading was functionally similar to that of BMP-2 administration in terms of phenotypic changes in the growth plate and endosteal mineralization. Histomorphometric analyses clearly showed that the number of osteoid osteocytes increased in response to mechanical loading, with similar tendencies observed for BMP-2 administration. Moreover, inhibition of BMP-Smad signaling attenuated cartilage and bone mineralization induced by mechanical stimulation or BMP-2 administration. Therefore, our data provide evidence that cartilage ossification and bone mineralization are regulated through at least partly the activation of the BMP-Smad signaling pathway by mechanical loading.

Furthermore, in response to mechanical loading, *Ihh*, *Col10a1*, and *Mmp13* (which regulate the development of hypertrophic chondrocyte and cartilage calcification in endochondral ossification), as well as the osteocyte markers *Dmp1*, *Phex*, and *Mepe* (regulators of mineralization and phosphate homeostasis) were upregulated in a load-dependent manner. These findings are in agreement with previous reports (Gluhak-Heinrich et al., 2003; Sundaramurthy and Mao, 2006; Harris et al., 2007; Kulkarni et al., 2010; Lin et al., 2010; Sergerie et al., 2011). In addition, the results of the present study, based on the *ex vivo* organ culture model, clarified that the long bone tissue-specific and mechanical loading-responsive genes and their gene expression patterns are largely influenced by the activation of BMP-Smad signaling following mechanical loading. Nevertheless, there could be numerous other pathways, including non-Smad pathways such as EGFR/ErbB signaling and the MAPK cascade, which are associated with mechanical loading, and their specific functions on bone mineralization *via* the identified genes and pathways should be validated by further investigations.

By analyzing the culture supernatant of the *ex vivo* samples, we also demonstrated that long bone mineralization is regulated by mechanical loading in the local environment, rather than systemically. Bone and cartilage metabolism and homeostasis are critically dependent on the local pH, and biomineralization occurs at alkaline pH (Arnett, 2008, 2010; Simao et al., 2013). pH also plays a pivotal role in regulating ALP activity and pyrophosphate levels (Chakkalakal et al., 1994; Wu et al., 1997; Simao et al., 2013). Moreover, mechanical loading enhances ALP activity (Guo et al., 2015; Wang et al., 2015), BMP induces ALP activity for mineralization (Takuwa et al., 1991; Rawadi et al., 2003; Salazar et al., 2016), and ALP activity is essential for calcification in cartilage and bone (Amizuka et al., 2012). However, prior to this study, there had been no evidence that mechanical loading regulates the extracellular fluid pH of long bones. In addition to confirming that ALP is activated in response to mechanical loading, we report for the first time that the pH of the organ culture supernatant became alkaline upon mechanical loading, indicating that mechanical loading may act as a pH regulator, resulting in a subsequent increase in ALP activity. We hypothesize that, *via* activation of the BMP-Smad pathway, mechanical loading alters the extracellular pH and thereby increases ALP activity to promote bone mineralization.

Microarray analysis revealed that endochondral ossification and bone mineralization-related genes were highly expressed under loading forces relative to non-loading. Surprisingly, however, *Car9* expression was markedly suppressed by mechanical loading. *Car9* encodes carbonic anhydrase IX, which is anchored in the plasma membrane. *Car9* may therefore regulate the pH of the extracellular environment of bone tissue. *Car9* downregulation can also induce *Col10a1* in hypertrophic chondrocytes (Maruyama et al., 2013). Further studies investigating *Car9* downregulation by mechanical loading are needed to clarify whether it is involved in promoting mineralization, and if so, the underlying mechanism.

The skeleton is maintained by regulation of the bone mineralization, which is dependent on a local balance between extracellular levels of ALP, Pi, and PPi (Sapir-Koren and Livshits, 2014a, 2014b; Orriss et al., 2016). Notably, for hydroxyapatite synthesis, it is essential that the optimal Pi/PPi ratio be maintained locally during bone growth (Thouverey et al., 2009; Sapir-Koren and Livshits, 2014a). Little is known regarding changes in the Pi/PPi ratio in the extracellular fluid in response to mechanical loading and how this change affects mineralization. In this study, we determined that the Pi/PPi ratio was higher in the loaded samples than the non-loaded samples, which may be one mechanism by which mechanical loading affects mineralization.

We recognize that our study has some limitations. First, as articular cartilage and growth plate damage in response to mechanical loading cannot be adequately evaluated using a normal or fluorescence microscope, detecting microfractures on injured cartilage in an *ex vivo* model will be addressed in the future. Second, as the surrounding tissue of the long bones was consistently removed and the organ culture model was isolated *ex vivo*, regulatory mechanisms associated with periosteal tissue or multiple organs in response to mechanical loading remain unclear. Therefore, the results should be confirmed in further studies. However, we have highlighted the mineralization-promoting mechanism within the long bone in response to mechanical loading using an *ex vivo*-specific, non-loading condition as a control. Third, as our gene expression data were obtained from whole long bones, the effects of mechanical loading on gene expression in localized areas of long bone are unknown. Therefore, further investigations into these critical molecules in response to mechanical loading, perhaps using laser capture microdissection and *in vivo* imaging, will be required to unravel their various roles in cartilage and bone mineralization and elucidate the mechanism of communication in osteocytes, osteoblasts, and osteoclasts. Given that long bones consist of mineralized bone, articular cartilage, bone marrow, and growth plate cartilage tissue, we suggest that *Car9* and other molecules may function in an opposite or reciprocal manner, concealing their differential actions on the diaphysis and epiphysis of the long bone.

In conclusion, the present study demonstrated that cyclic axial mechanical loading regulates endochondral ossification and endosteal mineralization in long bone development. The effects of mechanical loading can promote mineralization through at least partly the activation of BMP-Smad signaling, and loading alters the extracellular environment considerably. Therefore, analyzing the effects of mechanical loading could reveal key regulatory mechanisms influencing the mineralization of long bone development. This study also reports a novel *ex vivo* organ culture model, which may mimic endochondral ossification and endosteal mineralization in long bones *in vivo* under cyclic axial mechanical loading; it, thus, may be possible in the future to use this model to elucidate the mechanism of drugs that act synergistically with mechanical loading or substitute for mechanical stimulation.

CRediT authorship contribution statement

Conceptualization and methodology: SM; Formal analysis and investigation: SM and KN; Supervision and project administration: HY; Writing and approving the final version of manuscript: SM, HY and KN.

Transparency document

The Transparency document associated with this article can be found, in online version.

Declaration of competing interest

The authors declare that they have no known competing financial interests or personal relationships that could have appeared to influence the work reported in this paper.

Acknowledgements

We thank Akemi Ito and laboratory staff at the Ito Bone Histomorphometry Institute for help with histology preparations and suggestions for bone histomorphometry (Niigata, Japan). We also thank Hiroko Hagiwara at Microarray Laboratory of Cell Innovator Inc. (Fukuoka, Japan) at Kyushu University for help with microarray experiments and analysis. We thank Seiji Yamamoto in the Department of Pathology, Graduate School of Medicine and Pharmaceutical Science for Research, Graduate School of Innovative Life Science, University of Toyama (Toyama, Japan) for helpful comments and technical advice.

Funding

This research did not receive any specific grant from funding agencies in the public, commercial, or not-for-profit sectors.

Appendix A. Supplementary data

Supplementary data to this article can be found online at https://doi.org/10.1016/j.bonr.2021.101088.

References

Akamine, Y., Kakudo, K., Kondo, M., Ota, K., Muroi, Y., Yoshikawa, H., Nakata, K., 2012. Prolonged matrix metalloproteinase-3 high expression after cyclic compressive load on human synovial cells in three-dimensional cultured tissue. Int. J. Oral Maxillofac. Surg. 41, 874–881. https://doi.org/10.1016/j.ijom.2011.10.027.

Alberty, A., Peltonen, J., Ritsila, V., 1993. Effects of distraction and compression on proliferation of growth plate chondrocytes. A study in rabbits. Acta Orthop. Scand. 64, 449–455. https://doi.org/10.3109/17453679308993665.

Amizuka, N., Hasegawa, T., Oda, K., de Freitas, P.H.L., Hoshi, K., Li, M., Ozawa, H., 2012. Histology of epiphyseal cartilage calcification and endochondral ossification. Front. Biosci. (Elite Ed) 4, 2085–2100. https://doi.org/10.2741/526.

Arnett, T.R., 2008. Extracellular pH regulates bone cell function. J. Nutr. 138, 415s–418s. https://doi.org/10.1093/jn/138.2.415S.

Arnett, T.R., 2010. Acidosis, hypoxia and bone. Arch. Biochem. Biophys. 503, 103–109. https://doi.org/10.1016/j.abb.2010.07.021.
Baumann, A.P., Aref, M.W., Turnbull, T.L., Robling, A.G., Niebur, G.L., Allen, M.R., Roeder, R.K., 2015. Development of an in vivo rabbit ulnar loading model. Bone 75, 55–61. https://doi.org/10.1016/j.bone.2015.01.022.
Birkhold, A.I., Razi, H., Duda, G.N., Weinkamer, R., Checa, S., Willie, B.M., 2016. The periosteal bone surface is less mechano-responsive than the endocortical. Sci. Rep. 6, 23480. https://doi.org/10.1038/srep23480.
Bonewald, L.F., Johnson, M.L., 2008. Osteocytes, mechanosensing and Wnt signaling. Bone 42, 606–615. https://doi.org/10.1016/j.bone.2007.12.224.
Bries, A.D., Weiner, D.S., Jacquet, R., Adamczyk, M.J., Morscher, M.A., Lowder, E., Askew, M.J., Steiner, R.P., Horne, W.I., Landis, W.J., 2012. A study in vivo of the effects of a static compressive load on the proximal tibial physis in rabbits. J. Bone Joint Surg. Am. 94, e1111–e11110. https://doi.org/10.2106/JBJS.K.00340.
Chakkalakal, D.A., Mashoof, A.A., Novak, J., Strates, B.S., McGuire, M.H., 1994. Mineralization and pH relationships in healing skeletal defects grafted with demineralized bone matrix. J. Biomed. Mater. Res. 28, 1439–1443. https://doi.org/10.1002/jbm.820281209.
Chambers, S.M., Fasano, C.A., Papapetrou, E.P., Tomishima, M., Sadelain, M., Studer, L., 2009. Highly efficient neural conversion of human ES and iPS cells by dual inhibition of SMAD signaling. Nat. Biotechnol. 27, 275–280. https://doi.org/10.1038/nbt.1529.
De Luca, F., Barnes, K.M., Uyeda, J.A., De-Levi, S., Abad, V., Palese, T., Mericq, V., Baron, J., 2001. Regulation of growth plate chondrogenesis by bone morphogenetic protein-2. Endocrinology. 142, 430–436. https://doi.org/10.1210/endo.142.1.7901.
De Souza, R.L., Matsuura, M., Eckstein, F., Rawlinson, S.C.F., Lanyona, L.E., Pitsillides, A. A., 2005. Non-invasive axial loading of mouse tibiae increases cortical bone formation and modifies trabecular organization: a new model to study cortical and cancellous compartments in a single loaded element. Bone 37, 810–818. https://doi.org/10.1016/j.bone.2005.07.022.
Dexheimer, V., Gabler, J., Bomans, K., Sims, T., Omlor, G., Richter, W., 2016. Differential expression of TGF-beta superfamily members and role of Smad1/5/9-signalling in chondral versus endochondral chondrocyte differentiation. Sci. Rep. 6, 36655. https://doi.org/10.1038/srep36655.
Duneas, N., Crooks, J., Ripamonti, U., 1998. Transforming growth factor-beta 1: induction of bone morphogenetic protein genes expression during endochondral bone formation in the baboon, and synergistic interaction with osteogenic protein-1 (BMP-7). Growth Factors 15, 259–277. https://doi.org/10.3109/08977199809017482.
Gluhak-Heinrich, J., Ye, L., Bonewald, L.F., Feng, J.Q., MacDougall, M., Harris, S.E., Pavlin, D., 2003. Mechanical loading stimulates dentin matrix protein 1 (DMP1) expression in osteocytes in vivo. J. Bone Miner. Res. 18, 807–817. https://doi.org/10.1359/jbmr.2003.18.5.807.
Guo, Y., Wang, Y., Liu, Y., Wang, H., Guo, C., Zhang, X., 2015. Effect of the same mechanical loading on osteogenesis and osteoclastogenesis in vitro. Chin. J. Traumatol. 18, 150–156. https://doi.org/10.1016/j.cjtee.2014.09.004.
Harris, S.E., Gluhak-Heinrich, J., Harris, M.A., Yang, W., Bonewald, L.F., Riha, D., Rowe, P.S.N., Robling, A.G., Turner, C.H., Feng, J.Q., McKee, M.D., Nicollela, D., 2007. DMP1 and MEPE expression are elevated in osteocytes after mechanical loading in vivo: theoretical role in controlling mineral quality in the perilacunar matrix. J. Musculoskelet. Neuronal Interact. 7, 313–315. https://www.ncbi.nlm.nih.gov/pmc/articles/PMC3357082.
Iura, A., McNerny, E.G., Zhang, Y., Kamiya, N., Tantillo, M., Lynch, M., Kohn, D.H., Mishina, Y., 2015. Mechanical loading synergistically increases trabecular bone volume and improves mechanical properties in the mouse when BMP signaling is specifically ablated in osteoblasts. PLoS One 10, e0141345. https://doi.org/10.1371/journal.pone.0141345.
Keller, B., Yang, T., Chen, Y., Munivez, E., Bertin, T., Zabel, B., Lee, B., 2011. Interaction of TGFbeta and BMP signaling pathways during chondrogenesis. PLoS One 6, e16421. https://doi.org/10.1371/journal.pone.0016421.
Kopf, J., Petersen, A., Duda, G.N., Knaus, P., 2012. BMP2 and mechanical loading cooperatively regulate immediate early signalling events in the BMP pathway. BMC Biol. 10, 37. https://doi.org/10.1186/1741-7007-10-37.
Kulkarni, R.N., Bakker, A.D., Everts, V., Klein-Nulend, J., 2010. Inhibition of osteoclastogenesis by mechanically loaded osteocytes: involvement of MEPE. Calcif. Tissue Int. 87, 461–468. https://doi.org/10.1007/s00223-010-9407-7.
Kuruvilla, S.J., Fox, S.D., Cullen, D.M., Akhter, M.P., 2008. Site specific bone adaptation response to mechanical loading. J. Musculoskelet. Neuronal Interact. 8, 71–78.
Lin, Y.Y., Tanaka, N., Ohkuma, S., Iwabuchi, Y., Tanne, Y., Kamiya, T., Kunimatsu, R., Huang, Y.C., Yoshioka, M., Mitsuyoshi, T., Tanimoto, K., Tanaka, E., Tanne, K., 2010. Applying an excessive mechanical stress alters the effect of subchondral osteoblasts on chondrocytes in a co-culture system. Eur. J. Oral Sci. 118, 151–158. https://doi.org/10.1111/j.1600-0722.2010.00710.x.
Maruyama, T., Miyamoto, Y., Yamamoto, G., Yamada, A., Yoshimura, K., Suzawa, T., Takami, M., Akiyama, T., Hoshino, M., Iwasa, F., Ikumi, N., Tachikawa, T., Mishima, K., Baba, K., Kamijo, R., 2013. Downregulation of carbonic anhydrase IX promotes *Col10a1* expression in chondrocytes. PLoS One 8, e56984. https://doi.org/10.1371/journal.pone.0056984.
Ménard, A.L., Grimard, G., Valteau, B., Londono, I., Moldovan, F., Villemure, I., 2014. In vivo dynamic loading reduces bone growth without histomorphometric changes of the growth plate. J. Orthop. Res. 32, 1129–1136. https://doi.org/10.1002/jor.22664.
Moalli, M.R., Caldwell, N.J., Patil, P.V., Goldstein, S.A., 2000. An in vivo model for investigations of mechanical signal transduction in trabecular bone. J. Bone Miner. Res. 15, 1346–1353. https://doi.org/10.1359/jbmr.2000.15.7.1346.
Moustafa, A., Sugiyama, T., Saxon, L.K., Zaman, G., Sunters, A., Armstrong, V.J., Javaheri, B., Lanyon, L.E., Price, J.S., 2009. The mouse fibula as a suitable bone for the study of functional adaptation to mechanical loading. Bone 44, 930–935. https://doi.org/10.1016/j.bone.2008.12.026.
Muroi, Y., Kakudo, K., Nakata, K., 2007. Effects of compressive loading on human synovium-derived cells. J. Dent. Res. 86, 786–791. https://doi.org/10.1177/154405910708600819.
Niehoff, A., Kersting, U.G., Zaucke, F., Morlock, M.M., Bruggemann, G.P., 2004. Adaptation of mechanical, morphological, and biochemical properties of the rat growth plate to dose-dependent voluntary exercise. Bone 35, 899–908. https://doi.org/10.1016/j.bone.2004.06.006.
Ning, J., Zhao, Y., Ye, Y., Yu, J., 2019. Opposing roles and potential antagonistic mechanism between TGF-β and BMP pathways: implications for cancer progression. EbioMedicine 41, 702–710. https://doi.org/10.1016/j.ebiom.2019.02.033.
Ohashi, N., Robling, A.G., Burr, D.B., Turner, C.H., 2002. The effects of dynamic axial loading on the rat growth plate. J. Bone Miner. Res. 17, 284–292. https://doi.org/10.1359/jbmr.2002.17.2.284.
Orriss, I.R., Arnett, T.R., Russell, R.G., 2016. Pyrophosphate: a key inhibitor of mineralisation. Curr. Opin. Pharmacol. 28, 57–68. https://doi.org/10.1016/j.coph.2016.03.003.
Othman, H., Thonar, E.J., Mao, J.J., 2007. Modulation of neonatal growth plate development by ex vivo intermittent mechanical stress. J. Biomech. 40, 2686–2693. https://doi.org/10.1016/j.jbiomech.2006.12.014.
Quackenbush, J., 2002. Microarray data normalization and transformation. Nat. Genet. 32, 496–501. https://doi.org/10.1038/ng1032.
Rawadi, G., Vayssiere, B., Dunn, F., Baron, R., Roman-Roman, S., 2003. BMP-2 controls alkaline phosphatase expression and osteoblast mineralization by a Wnt autocrine loop. J. Bone Miner. Res. 18, 1842–1853. https://doi.org/10.1359/jbmr.2003.18.10.1842.
Robling, A.G., Duijvelaar, K.M., Geevers, J.V., Ohashi, N., Turner, C.H., 2001. Modulation of appositional and longitudinal bone growth in the rat ulna by applied static and dynamic force. Bone 29, 105–113. https://doi.org/10.1016/S8756-3282(01)00488-4.
Robling, A.G., Niziolek, P.J., Baldridge, L.A., Condon, K.W., Allen, M.R., Alam, I., Mantila, S.M., Gluhak-Heinrich, J., Bellido, T.M., Harris, S.E., Turner, C.H., 2008. Mechanical stimulation of bone in vivo reduces osteocyte expression of Sost/sclerostin. J. Biol. Chem. 283, 5866–5875. https://doi.org/10.1074/jbc.M705092200.
Salazar, V.S., Ohte, S., Capelo, L.P., Gamer, L., Rosen, V., 2016. Specification of osteoblast cell fate by canonical Wnt signaling requires Bmp2. Development 143, 4352–4367. http://dev.biologists.org/content/143/23/4352.abstract.
Sample, S.J., Collins, R.J., Wilson, A.P., Racette, M.A., Behan, M., Markel, M.D., Kalscheur, V.L., Hao, Z., Muir, P., 2010. Systemic effects of ulna loading in male rats during functional adaptation. J. Bone Miner. Res. 25, 2016–2028. https://doi.org/10.1002/jbmr.101.
Sapir-Koren, R., Livshits, G., 2014a. Bone mineralization is regulated by signaling cross talk between molecular factors of local and systemic origin: the role of fibroblast growth factor 23. BioFactors 40, 555–568. https://doi.org/10.1002/biof.1186.
Sapir-Koren, R., Livshits, G., 2014b. Osteocyte control of bone remodeling: is sclerostin a key molecular coordinator of the balanced bone resorption-formation cycles? Osteoporos. Int. 25, 2685–2700. https://doi.org/10.1007/s00198-014-2808-0.
Saunders, M.M., Simmerman, L.A., Reed, G.L., Sharkey, N.A., Taylor, A.F., 2010. Biomimetic bone mechanotransduction modeling in neonatal rat femur organ cultures: structural verification of proof of concept. Biomech. Model. Mechanobiol. 9, 539–550. https://doi.org/10.1007/s10237-010-0195-9DO.
Schreivogel, S., Kuchibhotla, V., Knaus, P., Duda, G.N., Petersen, A., 2019. Load-induced osteogenic differentiation of mesenchymal stromal cells is caused by mechano-regulated autocrine signaling. J. Tissue Eng. Regen. Med. 13, 1992–2008. https://doi.org/10.1002/term.2948.
Sergerie, K., Parent, S., Beauchemin, P., Londoño, I., Moldovan, F., Villemure, I., 2011. Growth plate explants respond differently to in vitro static and dynamic loadings. J. Orthop. Res. 29, 473–480. https://doi.org/10.1002/jor.21282.
Shimomura, K., Kanamoto, T., Kita, K., Akamine, Y., Nakamura, N., Mae, T., Yoshikawa, H., Nakata, K., 2014. Cyclic compressive loading on 3D tissue of human synovial fibroblasts upregulates prostaglandin E2 via COX-2 production without IL-1beta and TNF-alpha. Bone Joint Res. 3, 280–288. https://doi.org/10.1302/2046-3758.39.2000287.
Simao, A.M., Bolean, M., Hoylaerts, M.F., Millan, J.L., Ciancaglini, P., 2013. Effects of pH on the production of phosphate and pyrophosphate by matrix vesicles' biomimetics. Calcif. Tissue Int. 93, 222–232. https://doi.org/10.1007/s00223-013-9745-3DO.
Simmons, C.A., Alsberg, E., Hsiong, S., Kim, W.J., Mooney, D.J., 2004. Dual growth factor delivery and controlled scaffold degradation enhance in vivo bone formation by transplanted bone marrow stromal cells. Bone 35, 562–569. https://doi.org/10.1016/j.bone.2004.02.027.
Simske, S.J., Luttges, M.W., Wachtel, H., 1990. Age dependent development of osteopenia in the long bones of tail-suspended mice. Biomed. Sci. Instrum. 26, 87–94.
Sugiyama, T., Meakin, L.B., Browne, W.J., Galea, G.L., Price, J.S., Lanyon, L.E., 2012. Bones' adaptive response to mechanical loading is essentially linear between the low strains associated with disuse and the high strains associated with the lamellar/woven bone transition. J. Bone Miner. Res. 27, 1784–1793. https://doi.org/10.1002/jbmr.1599.
Sundaramurthy, S., Mao, J.J., 2006. Modulation of endochondral development of the distal femoral condyle by mechanical loading. J. Orthop. Res. 24, 229–241. https://doi.org/10.1002/jor.20024.

Tachi, K., Takami, M., Sato, H., Mochizuki, A., Zhao, B., Miyamoto, Y., Tsukasaki, H., Inoue, T., Shintani, S., Koike, T., Honda, Y., Suzuki, O., Baba, K., Kamijo, R., 2011. Enhancement of bone morphogenetic protein-2-induced ectopic bone formation by transforming growth factor-beta1. Tissue Eng. A 17, 597–606. https://doi.org/10.1089/ten.tea.2010.0094.

Takuwa, Y., Ohse, C., Wang, E.A., Wozney, J.M., Yamashita, K., 1991. Bone morphogenetic protein-2 stimulates alkaline phosphatase activity and collagen synthesis in cultured osteoblastic cells, MC3T3-E1. Biochem. Biophys. Res. Commun. 174, 96–101. https://doi.org/10.1016/0006-291X(91)90490-X.

Tatsumi, S., Ishii, K., Amizuka, N., Li, M., Kobayashi, T., Kohno, K., Ito, M., Takeshita, S., Ikeda, K., 2007. Targeted ablation of osteocytes induces osteoporosis with defective mechanotransduction. Cell Metab. 5, 464–475. https://doi.org/10.1016/j.cmet.2007.05.001.

Thouverey, C., Bechkoff, G., Pikula, S., Buchet, R., 2009. Inorganic pyrophosphate as a regulator of hydroxyapatite or calcium pyrophosphate dihydrate mineral deposition by matrix vesicles. Osteoarthr. Cartil. 17, 64–72. https://doi.org/10.1016/j.joca.2008.05.020.

Tu, X., Rhee, Y., Condon, K., Bivi, N., Allen, M.R., Dwyer, D., Stolina, M., Turner, C.H., Robling, A.G., Plotkin, L.I., Bellido, T., 2012. Sost downregulation and local Wnt signaling are required for the osteogenic response to mechanical loading. Bone 50, 209–217. https://doi.org/10.1016/j.bone.2011.10.025.

Turner, C.H., Akhter, M.P., Raab, D.M., Kimmel, D.B., Recker, R.R., 1991. A noninvasive, in vivo model for studying strain adaptive bone modeling. Bone 12, 73–79. https://doi.org/10.1016/8756-3282(91)90003-2.

Villanueva, A.R., Frost, H.M., 1961. A rapid method for obtaining hematoxylin and eosin biopsy sections of bone for table diagnosis. Am. J. Clin. Pathol. 36, 54–59. https://doi.org/10.1093/ajcp/36.1.54.

Wang, L., Zhang, X., Guo, Y., Chen, X., Li, R., Liu, L., Shi, C., Guo, C., Zhang, Y., 2010. Involvement of BMPs/Smad signaling pathway in mechanical response in osteoblasts. Cell. Physiol. Biochem. 6, 1093–1102. https://doi.org/10.1159/000323987.

Wang, Q.S., Zhang, X.C., Li, R.X., Sun, J.G., Su, W.H., Guo, Y., Li, H., Zhang, X.Z., 2015. A comparative study of mechanical strain, icariin and combination stimulations on improving osteoinductive potential via NF-kappaB activation in osteoblast-like cells. Biomed. Eng. Online 14, 46. https://doi.org/10.1186/s12938-015-0039-z.

Wang, X., Mao, J.J., 2002. Accelerated chondrogenesis of the rabbit cranial base growth plate by oscillatory mechanical stimuli. J. Bone Miner. Res. 17, 1843–1850. https://doi.org/10.1359/jbmr.2002.17.10.1843.

Weatherholt, A.M., Fuchs, R.K., Warden, S.J., 2013. Cortical and trabecular bone adaptation to incremental load magnitudes using the mouse tibial axial compression loading model. Bone 52, 372–379. https://doi.org/10.1016/j.bone.2012.10.026.

Wu, L.N., Genge, B.R., Dunkelberger, D.G., LeGeros, R.Z., Concannon, B., Wuthier, R.E., 1997. Physicochemical characterization of the nucleational core of matrix vesicles. J. Biol. Chem. 272, 4404–4411. https://doi.org/10.1074/jbc.272.7.4404.

Zhang, P., Su, M., Tanaka, S.M., Yokota, H., 2006. Knee loading stimulates cortical bone formation in murine femurs. BMC Musculoskelet. Disord. 7, 73. https://doi.org/10.1186/1471-2474-7-73.

Zhang, P., Su, M., Liu, Y., Hsu, A., Yokota, H., 2007. Knee loading dynamically alters intramedullary pressure in mouse femora. Bone 40, 538–543. https://doi.org/10.1016/j.bone.2006.09.018.

Zhang, P., Turner, C.H., Yokota, H., 2009. Joint loading-driven bone formation and signaling pathways predicted from genome-wide expression profiles. Bone 44, 989–998. https://doi.org/10.1016/j.bone.2009.01.367.